Title

Injectable hyaluronic acid based microrods provide local micromechanical and biochemical cues to attenuate cardiac fibrosis after myocardial infarction.

Authors

Le, Long V
Mohindra, Priya
Fang, Qizhi
et al.

Publication Date

2018-07-01

DOI

10.1016/j.biomaterials.2018.03.042

Peer reviewed

HHS Public Access

Author manuscript

Biomaterials. Author manuscript; available in PMC 2019 July 01.

Published in final edited form as:

Biomaterials. 2018 July ; 169: 11–21. doi:10.1016/j.biomaterials.2018.03.042.

Injectable hyaluronic acid based microrods provide local micromechanical and biochemical cues to attenuate cardiac fibrosis after myocardial infarction

Long V. Le[a], **Priya Mohindra**[a], **Qizhi Fang**[b], **Richard E. Sievers**[b], **Michael Mkrtschjan**[c], **Christopher Solis**[d], **Conrad W. Safranek**[e], **Brenda Russell**[d], **Randall J. Lee**[a,b], and **Tejal A. Desai**[a,e]

[a]UC Berkeley-UCSF Graduate Program in Bioengineering, University of California, San Francisco, San Francisco, CA, 94158

[b]Department of Medicine, University of California, San Francisco, San Francisco, CA, 94143

[c]Department of Bioengineering, University of Illinois, Chicago, Chicago, IL, 60607

[d]Department of Physiology and Biophysics, University of Illinois, Chicago, Chicago, IL, 60612

[e]Department of Bioengineering and Therapeutic Sciences, University of California, San Francisco, San Francisco, CA, 94158

Abstract

Repairing cardiac tissue after myocardial infarction (MI) is one of the most challenging goals in tissue engineering. Following ischemic injury, significant matrix remodeling and the formation of avascular scar tissue significantly impairs cell engraftment and survival in the damaged myocardium. This limits the efficacy of cell replacement therapies, demanding strategies that reduce pathological scarring to create a suitable microenvironment for healthy tissue regeneration. Here, we demonstrate the successful fabrication of discrete hyaluronic acid (HA)-based microrods to provide local biochemical and biomechanical signals to reprogram cells and attenuate cardiac fibrosis. HA microrods were produced in a range of physiological stiffness and shown to degrade in the presence of hyaluronidase. Additionally, we show that fibroblasts interact with these microrods *in vitro*, leading to significant changes in proliferation, collagen expression and other markers of a myofibroblast phenotype. When injected into the myocardium of an adult rat MI model, HA microrods prevented left ventricular wall thinning and improved cardiac function at 6 weeks post infarct.

Keywords

Tissue engineering; Biomaterials; Mechanotransduction; Cardiovascular disease; Photolithography

Corresponding Author Tejal A. Desai, 1700 4th St Rm 204, San Francisco, CA 94158-2330, 415-514-9695, tejal.desai@ucsf.edu.

2. Introduction

Ischemic heart disease is the leading cause of death worldwide, accounting for 16% of total deaths in 2015 [1]. While advancements in preventive and acute treatment of myocardial infarctions (MI) have improved patient outcomes and reduced mortality rates, the resulting tissue damage initiates pathological repair mechanisms that culminate in the formation of non-contractile scar tissue. This progressive tissue stiffening results in additional stress on the heart and reduces cardiac output [2–4]. Currently, the lack of treatment for this maladaptive response leads to challenging chronic complications and eventual heart failure in a growing patient population.

Within the past 5 years, there have been significant efforts towards developing intramyocardial hydrogel injections for cardiac tissue repair after MI [5–9]. These hydrogels act as bulking agents to thicken and mechanically stabilize the damaged myocardium, decreasing left ventricle (LV) wall stress and limiting LV expansion. While a multitude of materials have been investigated, injectable hyaluronic acid (HA) hydrogels have gained increasing attention for cardiac tissue regeneration due to the implications of HA in wound healing [10–15].

HA is a naturally derived polysaccharide that is produced and degraded by many cell types [16–19]. As a critical component of the ECM, HA plays roles in a range of biological processes, including angiogenesis and inflammation [17,20,21]. Accordingly, many HA-based scaffolds have been developed within the past decade to exploit these advantageous properties [22,23]. While bulk HA injections have seen success in preclinical studies, there remain significant challenges that limit their clinical feasibility and efficacy.

We have previously used polymeric microrods and microfibers to act as anchors for fibroblasts to mitigate the fibrotic phenotype [24–26]. This mechanobiology approach is a promising strategy for locally reducing the formation of scar tissue without the need for soluble drugs, eliminating concerns related to systemic side effects and drug release kinetics. To date, there are no existing therapeutic strategies utilizing hyaluronic acid in a microstructure-based approach for cardiac tissue regeneration *in vivo*. Here, we demonstrate the development and application of injectable hyaluronic acid-based microrods for comprehensive cardiac repair after MI. These HA-based microrods are biodegradable, promote cell growth, attenuate the myofibroblast phenotype and preserve myocardial structure and function after MI.

3. Results

3.1 Optimization of hyaluronic acid based microrods

In order to fabricate hyaluronic acid microrods through photolithography, we adapted published protocols to functionalize HA with UV-sensitive methacrylate groups (Figure 1A) [27]. ^{1}H NMR spectroscopy confirmed the substitution of hydroxyls with methacrylate groups, showing methacrylate peaks at 6.1 and 5.65 ppm (Figure 1B). To determine the degree of substitution, we compared the integrations of the methacrylate peaks with the

acetamide peak in HA at 1.85 ppm and found that we were able to reproducibly synthesize hyaluronic acid methacrylate (HAMA) with 41 ± 3% substitution.

We have previously found that microrods must have an elastic modulus of at least 20 kPa in order to significantly affect cell behavior [26]. To determine the concentration of HAMA necessary to yield microrods of desired stiffness, we measured the elastic modulus of hydrogel slabs fabricated with a range of HAMA concentrations. Atomic force microscopy measurements showed that the modulus of these hydrogels increase exponentially from 1kPa to 160kPa with increasing HAMA concentration (Figure 1C). For later studies, we used 75 mg/mL and 100 mg/mL HAMA concentrations to fabricate microrods with Young's moduli of 70 kPa and 160 kPa, respectively.

Photolithography was used to reproducibly create 15 × 15 × 100 μm HA microrods in a range of stiffness (Figure 2A). The dimensions of the microrods were controlled by the photomask while the stiffness was controlled by total HAMA concentration in the precursor solution. Brightfield microscopy confirmed uniform fabrication of HA microrods across the wafer (Figure 2B). Since HA is very hygroscopic, the fabricated HA microrods exhibit moderate swelling in solution. The dimensions of fully swollen HA microrods were confirmed by labeling HA microrods with a fluorescein label and imaging with confocal microscopy (Figure 2C).

3.2 Degradation kinetics of hyaluronic acid microrods

We conducted degradation studies on slabs of HAMA to understand the behavior of HAMA breakdown. Slabs of HAMA at varying concentration were incubated in buffer containing 100 U/mL, 10 U/mL and 0 U/mL of hyaluronidase. Samples were taken every two days and the degradation buffer was replenished. A carbazole-based detection assay was used to quantify the amount of HA released by degradation [28]. In samples incubated with 100 U/mL of hyaluronidase, 25 mg/mL and 50 mg/mL HAMA slabs degraded quickly and were completely disintegrated at 2 and 4 days, respectively (Figure 3A). As HAMA concentration increased, degradation was much slower, as seen in the 75 mg/mL and 100 mg/mL slabs, which did not completely degrade until after 3 weeks. This can be attributed to the increasing number of crosslinks that can be formed at higher HAMA concentrations, as observed with the nonlinear increases in elastic modulus with increasing HAMA. This results in a tighter mesh network in which only HAMA fragments on the surface are accessible to hyaluronidase. This is consistent with our observation that 75 and 100 mg/mL HAMA slabs became smaller in size, but maintained their mechanical integrity (Supplemental Figure 1A). By contrast, 25 and 50 mg/mL HAMA slabs became softer over a short period of time and then fully dissolved.

To confirm this, we compared degradation of 100 mg/mL HAMA slabs in 100 U/mL and 10 U/mL hyaluronidase. Not surprisingly, we found that slabs in 10 U/mL hyaluronidase degraded much slower than those in 100 U/mL hyaluronidase (Figure 3B, Supplemental Figure 1B). However, at two weeks, the rate of degradation for both groups became nearly identical. This suggests that there is an initial phase where there are many accessible HAMA fragments and degradation is dependent on hyaluronidase concentration; and that there is a second phase where the rate limiting factor is the number of accessible HAMA fragments on

the surface of the slab. We propose that hydrolysis of the crosslinks, which occurs much slower than enzyme mediated chain scission, loosens the polymer network and is the limiting step in this phase of degradation. This suggests that geometry may be a major factor in determining degradation time, so we proceeded to repeat these studies with HA microrods.

HA microrods were made using 75 mg/mL and 100 mg/mL of HAMA and incubated in buffer containing hyaluronidase, as described above. Samples were taken every two days and measured using the carbazole assay. Interestingly, we find that there is no significant difference between the degradation of 75 mg/mL and 100 mg/mL HA microrods (Figure 3C). The surface area to volume ratio of HA microrods is much greater than HAMA slabs, exposing more HAMA fragments to enzyme for degradation. As a result, the degradation of the HA microrods is also much faster than the HAMA polymer slabs. The 75 mg/mL and 100 mg/mL HA microrods were 50% degraded by 1 and 2 days, respectively, compared to their HAMA slab counterparts which were 50% degraded by 3 and 6 days (Supplemental Figure 1C). Differential interference contrast (DIC) imaging showed that these microrods degrade by surface erosion (Figure 3D).

3.3 Influence of hyaluronic acid microrods on fibroblasts and myocytes in vitro

We grew fibroblasts with HA microrods to evaluate the effect of HA microrods on fibroblast behavior *in vitro*. Primary neonatal rat ventricular fibroblasts (NRVFs) adhered to and spread on the HA microrods, often conforming to and enveloping the entirety of the rod (Figure 4A–B). Paxillin staining showed that the NRVFs formed distinct focal adhesions to the edges of the microrods, potentially initiating several mechanotransduction pathways. We show that fibronectin binds to the HA microrods to mediate this interaction in fibroblast/myocyte co-culture (Supplemental Figure 2). While a key binding partner to HA, CD44 was not found to be localized to the HA microrod and was instead present over the entire fibroblast membrane (Supplemental Figure 3), suggesting that CD44 is not mediating these physical interactions.

Interestingly, interaction with HA microrods increased fibroblast proliferation when cultured over three days (Figure 4E). NIH-3T3 fibroblasts grown with HA microrods in a 1:5 ratio of microrods:cells had increased proliferation rates compared to control cells grown on tissue culture plastic ($p < 0.01$). This contrasts with previous studies using PEG-based microrods, which reduced fibroblast proliferation [26]. This can be attributed to HA having additional cell growth properties compared to PEG, which is considered relatively bioinert. Despite the increased proliferation of fibroblasts, gene expression studies showed a decrease in key fibrosis markers. In cells grown with HA microrods, there was a dose-dependent decrease in expression of collagen I (Col1A2) and alpha smooth muscle actin (αSMA), markers of a myofibroblast phenotype. (Figure 4F). In cells cultured in a 1:20 ratio of rods:cells, Col1A2 expression was reduced to 0.31 ± 0.04 fold expression relative to cells grown without microrods ($p < 0.001$) while αSMA was reduced to 0.09 ± 0.02 fold expression ($p < 0.001$). This effect was more profound when the number of rods was increased to 1 per 5 cells. Additionally, HA microrods significantly reduced TGFβ1 expression and Smad3 expression (Figure 4G, $p < 0.05$). These data suggest that the HA microrods act on the TGFβ-signaling

pathway to reduce the myofibroblast phenotype. We further examined the effect of HA microrods on the expression of matrix metalloproteinases (MMPs), specifically MMP2 and MMP9. These MMPs are upregulated following myocardial infarction to facilitate the initial breakdown and remodeling of ECM. We found that MMP2 was significantly reduced in fibroblasts cultured with HA microrods compared to control cells (Figure 4H, $p < 0.05$), suggesting that HA microrods may attenuate aberrant ECM breakdown during the initial days after MI.

Neonatal rat ventricular myocytes (NRVMs) were grown with HA in solution or HA microrods for 48 hours to elucidate their effects on cardiomyocytes. Kymographs were derived from line scans under DIC illumination to determine the beats per minute and time to peak tension (Supplemental Figure 4) [29]. No significance was found between groups, suggesting that neither HA microrods nor free HA interfere with the contractile properties of the NRVMs.

Taken together, these results suggest that HA microrods show promise as a therapeutic strategy to promote regenerative processes in the infarcted myocardium while mitigating pathological scarring.

3.4 Influence of hyaluronic acid microrods in vivo

An infarct was induced in rats by ischemia reperfusion to generate a cardiac fibrosis model. After 48 hours, HA microrods, soluble HA or saline were delivered into the infarct zone by ultrasound-guided, transthoracic injection. Total HA mass was kept equal for soluble HA and HA microrod injections to account for the material effect of HA. After six weeks, the rats were sacrificed and hearts were harvested and fresh frozen for histological analyses. Cryosections of heart tissue were stained with hematoxylin and eosin (H&E), Masson's trichrome and Picrosirius red to evaluate the effect of microrod injection on the progression of cardiac fibrosis, as compared to injections of soluble HA or saline (Figure 5A).

Wall thickness measurements were performed on sections throughout the heart where the left ventricle cavity was visible. The left ventricular wall of hearts treated with HA microrods had greater minimum wall thickness (1.22 ± 0.38 mm) compared to saline treated hearts (0.70 ± 0.24 mm), which exhibited significant wall thinning ($p < 0.05$, Figure 5B). Animals treated with HA solution had moderate wall thinning compared to saline treated and HA microrod treated hearts (1.03 ± 0.21 mm). Heart sections were then stained with Masson's trichrome and Picrosirius red to quantify the size and collagen content of the infarcts. A comparison of rats treated with HA microrods or soluble HA to those treated with saline showed moderate, although not significant, reduction in collagen deposition in the free wall of the left ventricle ($p = 0.1$, Supplemental Figure 5).

These morphological improvements also translated to improved functional outputs. At 6 weeks, stroke volume was significantly greater in animals treated with HA microrods compared to animals treated with saline ($p < 0.01$, Supplemental Figure 6C). Change in ejection fraction (EF) was determined by taking the difference in ejection fraction measured at 2 days (before injection) and 6 weeks. Rats treated with HA microrods have a positive improvement in ejection fraction (5.91% ± 3.67%) compared to HA solution controls

(−0.36% ± 4.20%, $p < 0.05$) and saline controls (−8.22% ± 7.28%, $p < 0.001$). Animals treated with soluble HA also exhibited significant improvements in ejection fraction compared to saline ($p < 0.01$), suggesting beneficial effects from the material alone. There was no significant difference in left ventricular end diastolic volume (LSEDV) and left ventricular end systolic volume (LVESV) (Supplemental Figure 6A–B).

Examining the HA microrod injection area, we noted that the collagen deposited around the microrods was much less dense and not visible under polarized light, suggesting a local decrease in collagen deposition and maturation (Figure 6A–E). Immunofluorescence staining with markers of vimentin for fibroblasts and CD68 for macrophages indicated that both CD68-positive macrophages and vimentin-positive, CD68-negative fibroblasts were present at the injection site (Supplemental Figure 7A). Additionally, we found that fibroblasts surrounding the HA microrods had more rounded nuclei compared to those found away from the injection site, which were spindle shaped and characteristic of activated myofibroblasts (Supplemental Figure 7B). Immunofluorescent staining of actin and paxillin also showed that cells within the injection site interacted with the HA microrods and formed focal adhesions along the edges of the rods (Figure 6F–I). It is likely that this interaction locally reduces fibroblast activation *in vivo* as was seen *in vitro*.

4. Discussion

In this work, we developed a novel materials-based strategy that combines the wound healing properties of hyaluronic acid with microtopographical cues to attenuate the fibrotic phenotype and encourage the repair of damaged cardiac tissue after MI. We fabricated discrete microrods using a photocrosslinkable derivative of HA, characterized their enzyme-mediated degradation, and demonstrated localized anti-fibrotic effects using *in vitro* and *in vivo* models.

Previous studies have utilized bulk HA injections to mechanically support the damaged myocardium and preserve cardiac function after MI [10–15]. These strategies typically use biocompatible crosslinking chemistries to form the HA hydrogel *in situ*. While this allows for noninvasive catheter-based delivery, the gelation kinetics of HA in these cases can present significant challenges. Rapid gelation can lead to clogging of the catheter during the multiple injections required for treatment, while slow gelation results in diffusion of the hydrogel material into the tissue, leading to compromised hydrogel structure and mechanical properties [30–32]. Utilizing a rigorous interdisciplinary approach, we developed HA microrods to overcome these limitations. These discrete microstructures were fully crosslinked and characterized before injection and can be delivered to the myocardial wall by catheter injection without risk of clogging. Additionally, the ability to crosslink prior to injection gives tighter control over cell shaped morphology and hydrogel stiffness in the physiologic range, which are both crucial properties for mechanotransduction [33–35].

Within the past several decades, mechanical signaling has gained appreciation as a powerful mechanism for controlling cell behavior [33–41]. This includes mechanical stiffness, shear forces and topography. In contrast to bulk polymer injections that reduce wall stress by providing mechanical support and preventing LV dilation, discrete HA microrods provide

local micromechanical and biochemical signals to reprogram the cells of the myocardium. We have used both polypropylene microfibers and polyethylene glycol (PEG) microstructures to supply external mechanical cues and reduce myofibroblast differentiation [24–26]. HA microrods were shown to attenuate the fibrotic response to a greater degree than previously developed materials, likely due to the added biochemical effects of HA (Figure 4E,F). Chopra *et al* reported the role of HA in enhancing integrin mediated mechanotransduction [42]. Mesenchymal stem cells and fibroblasts were able to anchor to soft HA hydrogels containing fibronectin and observed increased rates of proliferation compared to soft polyacrylamide gels with fibronectin. Our cell proliferation data are consistent with these results, suggesting that the pro-proliferative effects of HA are preserved. Additionally, expression of key myofibroblast markers, αSMA and collagen 1, were reduced in NIH-3T3 fibroblasts to a greater extent compared to our studies with PEG microrods, an inert microtopographic cue [26].

The results of our *in vivo* experiments support these observations as well. The introduction of HA microrods 2 days after the initial infarct provides anchors for fibroblasts, macrophages and other cell types. Cells found at the injection site interacted with the microrods through focal adhesions, likely due to the increased stiffness relative to surrounding tissue (Figure 6F–I). We propose that this stiffness differential leads to attenuation of the myofibroblast phenotype, manifesting in decreased deposition of collagen, reduced wall thinning and improved cardiac output. Similar to our *in vitro* results, HA microrods improved LV ejection fraction (5.91% ± 3.67%) to a greater degree as compared to previous studies using PEG microrods (−2.59% ± 8.11%) [24]. At 6 weeks, cardiac function of HA microrod treated hearts surpassed baseline, post-infarct function, highlighting the potential of this technology to promote endogenous repair mechanisms not previously seen in materials-based approaches. We investigated whether this was due solely to the biological effect of HA by injecting a solution of HA into the heart wall after MI. The concentrations used were not high enough to generate a stiff gel, yet there were also improvements on cardiac function (Figure 5C). This is likely due to the wound healing properties of HA, which may contribute to the results seen in studies involving bulk HA injections [20–22,43].

We originally hypothesized that fibroblasts bind to HA microrods via CD44 receptors on the cell surface, activating a sequence of signaling cascades that induce phenotypic changes. Fibroblasts display a high content of CD44 receptor and conform well to the microrod topography, suggesting that fibroblasts are responsive to HA microrods in the local environment (Supplemental Figure 3). However, both myocytes and fibroblasts exhibit focal adhesions to the HA microrod contour (Figures 4A–D, Supplemental Fig 3). The deposition of fibronectin to HA explains how cells are able to attach to HA, a material that is traditionally believed to be nonadhesive (Supplemental Figure 2). This is consistent with previous reports that HA is nonadherent during the first few hours of culture, but becomes adherent and amenable to cell attachment after several hours have passed [44]. One possibility is that CD44 facilitates fibroblast association with the HA microrods, promoting altered gene expression levels (Figure 4F) while fibronectin supports continuous attachment [45]. Additionally, it has been shown that modification of the HA backbone can reduce its affinity for CD44 [46]. It is possible that our ~41% modification of the 6C-OH is sufficiently

high that it impairs the affinity of CD44 on the cell surface to the HA microrods. We therefore hypothesize that integrin binding is a key mechanism of interaction between fibroblasts and HA microrods, which may be amplified by other pathways involving HA and resulting in greater attenuation of the fibrotic phenotype. Additional investigation is necessary to elucidate the precise interactions and mechanisms for these phenotypic changes.

A significant advantage of HA microrods is that they are degradable by native physiological processes [17,19,21,22,43,47,48]. After attenuating the fibrotic response in the first few days after injection, these microrods degrade after several months to accommodate new tissue growth. While several studies have investigated the degradation behavior of covalently crosslinked HA hydrogels, it is necessary to characterize each new formulation since molecular weight, degree of methacrylation and weight percent can drastically affect degradation. In our study, we use lower molecular weight HA in our synthesis to achieve high degrees of methacrylation (Figure 1B). Additionally, we can get higher concentrations of low molecular weight HA (LMWHA) compared to high molecular weight HA (HMWHA), allowing for fabrication of hydrogels in a greater range of stiffness (Figure 1C). We used varying concentrations of hyaluronidase to understand the behavior of this degradation. For 100 mg/mL HA hydrogels, we observed an initial linear phase of degradation that was dependent on concentration of hyaluronidase (Figure 3B). This was followed by a second slow phase of degradation that was independent of hyaluronidase concentration. These data suggest that these HA hydrogels are first degraded through an enzyme mediated mechanism which break up the accessible HA chains on the surface of the hydrogels. When there is high crosslinking density, the enzyme will only degrade the exterior of the hydrogel, resulting in surface erosion. In contrast, looser hydrogel networks allow the enzyme to penetrate the interior and cause bulk degradation. This is also apparent by morphological analysis wherein lower weight percent HA hydrogels gradually lost mechanical integrity and eventually completely dissolved, while higher percent HA hydrogels became smaller over time, indicating surface degradation.

The goal of this study was to design and fabricate microstructures that can treat the progression of cardiac fibrosis post-MI to improve functional outcomes. These HA microrods act through mechanotransduction pathways to reduce fibrosis and maintain the structural integrity of the myocardium. Additionally, crosslinked HA can be compared to high molecular weight HA, which has anti-inflammatory effects that can limit pathological ECM remodeling during the initial days after an infarct [43,49,50]. Throughout degradation, these HA microrods are expected to release HA oligosaccharides that have been demonstrated to promote wound healing [51]. While it is difficult to investigate and tune the temporal interplay of mechanotransduction pathways and biochemical HA signaling pathways, our findings demonstrate that these two modes of action have significant implications for cardiac regeneration. By probing these individual pathways and responses, we will be able to optimize this novel microstructure-based technology to initially reduce the aberrant fibrotic response with micromechanical cues and later stimulate vascularization and other endogenous repair mechanisms for comprehensive myocardial repair.

5. Conclusions

Our acellular microrod approach is unique and provides biodegradable and bioactive micromechanical signals to directly limit fibrosis and favorably influence the microenvironment to attenuate myocardial wall thinning and improve LV function. These microrods were produced in a range of physiologically relevant stiffness and are able to degrade in the presence of natural enzymes. Introduction of these microrods to the injured heart provided anchors to surrounding cells during initial inflammatory processes when the ECM is being degraded. This micromechanical interaction attenuated the fibrotic phenotype and improved morphological and functional outcomes in a rat ischemia-reperfusion model of MI. In the future, this innovative strategy can be co-implemented with pharmacologic and cell-based therapies to further advance our limited clinical capabilities in treating the chronic complications of MI.

7. Materials and Methods

7.1 Synthesis of hyaluronic acid methacrylate

Hyaluronic acid methacrylate was synthesized based on a method published by Bencherif *et al* [27]. Briefly, sodium hyaluronate (100 kDa) was dissolved in a solution of 1:1 deionized water:dimethylformamide at 3.75 mg/mL. A 100-fold molar excess of glycidyl methacrylate and 35-fold molar excess of triethylamine was then added. The reaction was allowed to proceed for 24 hours at room temperature and away from light. Hyaluronic acid and hyaluronic acid methacrylate were recovered by precipitation in an excess of isopropanol. The precipitate was then pelleted by centrifugation at 700 × *g* for 5 minutes and dissolved in 50 mL of water. The resulting solution was dialyzed against water for 48 hours with three changes and lyophilized for 3 days at −40°C and 65 mtorr to yield a dry powder. Degree of methacrylation was determined by ^{1}H-NMR in D_2O using a Bruker Avance III HD 400 NMR.

7.2 Microrod fabrication

Hyaluronic acid methacrylate was dissolved in DI water containing 0.5% w/v of 2-hydroxy-4′-(2-hydroxyethoxy)-2-methylpropiophenone. Once fully dissolved, the solution was centrifuged at max speed for 5 minutes to remove impurities. A 15 μm thick layer of this solution was deposited onto a piranha cleaned silicon wafer and exposed through a photomask to a 365 nm UV light source using a Karl Suss Mask Aligner to crosslink the hyaluronic acid methacrylate in rod shapes (15 μm × 100 μm). The microrods were then gently scraped off the surface of the wafer using a cell scraper and collected into water, where uncrosslinked regions of hyaluronic acid methacrylate would fully dissolve. The microrods were passed through a 150 μm mesh filter to remove large particles and washed thoroughly by centrifugation. The microrods are sterilized with 70% ethanol and resuspended in saline or cell culture medium prior to use. Microrods were imaged using differential interference contrast (DIC). To visualize 3D geometry, HA microrods were labeled with 4′-(aminomethyl)fluorescein (Thermofisher, Waltham, MA) through EDC/NHS coupling and imaged using confocal microscopy.

7.3 Characterization of hyaluronic acid methacrylate stiffness

Crosslinked hyaluronic acid methacrylate hydrogels were fabricated in a range of concentrations. The stiffness of these hydrogels was determined by atomic force microscopy using a MFP3D-BIO inverted optical AFM (Asylum Research) mounted on a Nikon TE2000-U inverted fluorescent microscope. For these measurements, a gold deposited silicon nitride cantilever (k = 0.09 N/m) with a pyramidal tip was used. 10 measurements were made for each hydrogel at 3 different locations. The average of these 30 measurements was used for each replicate. Cantilevers were calibrated using a thermal oscillation method prior to each session.

7.4 Degradation of crosslinked hyaluronic acid methacrylate

Crosslinked hyaluronic acid methacrylate hydrogels were degraded at 37°C in 100 U/mL or 10 U/mL hyaluronidase. A phosphate buffered saline condition was used as a control to evaluate hydrolysis mediated degradation. The supernatant for each hydrogel was collected and replaced with fresh buffer solution every 48 hours. For each time point, the amount of uronic acid was measured using a carbazole based reaction [28]. Briefly, 200 μl of 24 mM sodium tetraborate decahydrate dissolved in concentrated sulfuric acid was added to 50 ul of each sample and heated to 100°C for 10 minutes. 50 μl of 0.125% carbazole in absolute ethanol was then added to each sample and heated to 100°C for 15 minutes. 200 ul of each solution was analyzed in a plate reader at 530 nm. Standard solutions of known concentrations of 100 kDa HA were used as a standard. Following the last time point, all remaining hydrogels were placed in concentrated sulfuric acid and assayed to determine the total amount of HA remaining.

For HA microrods, degradation was conducted by incubating the microrods in 100 U/mL, 10 U/mL and 0 U/mL hyaluronidase at 37°C. The microrods were pelleted by centrifugation at maximum speed for 5 minutes. The supernatant was collected and replaced with fresh buffer solution. Uronic acid was quantified as described above.

7.5 Cell culture and qPCR

NIH 3T3 mouse fibroblasts (ATCC, Manassas, Virginia) were cultured in the complete medium consisting of Dulbecco’s modified Eagle’s medium with 10% fetal bovine serum and 1% penicillin/streptomycin. Cells were harvested and cultured with HA microrods (100 mg/mL) at a high ratio (1:5) or a low ratio (1:20) of microrods to cells. Cell proliferation was assessed at 24, 48 and 72 hours after initial seeding using a CyQUANT assay. Experiments were done in triplicate. Genetic material was harvested and purified using the RNeasy Miniprep kit. RNA was converted into cDNA using the iScript cDNA synthesis kit (Bio-Rad Laboratories, Hercules, CA). A Viia7 qPCR machine (Life Technologies, Carlsbad, CA) was used to measure relative expression levels of gene targets as compared to a housekeeping gene. Expression levels of all genes were evaluated using SYBR Green Mastermix (Life Technologies, Grand Island, NY) and custom-made DNA primers (Integrated DNA Technologies, Coralville, IA) in triplicate for three biological replicates (See Supplementary Table 1).

7.6 Neonatal rat ventricular myocyte (NRVM) and fibroblast (NRVF) culture

Primary heart cultures were obtained from neonatal rats according to Institutional and National Institutes of Health guidelines. Hearts were removed from 1- to 2-day-old Sprague-Dawley rats and cells isolated using collagenase type II (Worthington Biochemical, Lakewood, NJ), per previously established protocol [52]. Fibroblasts, which had been separated from myocytes during isolation, were cultured an additional 2 days before detaching cells with trypsin and seeding in new dishes for experiments.

7.7 Kymograph analysis of cardiomyocyte contractility

Neonatal ventricular cardiomyocytes were plated on fibronectin-coated dishes (10 μg/mL) or fibronectin-coated dishes with HA previously deposited (10,000 HA rods/dish). A subset of dishes were chronically exposed to hyaluronic acid (0.042 mg) starting on the plating day. On the second day of incubation, kymographs derived from line scans with DIC illumination were used to derive cardiomyocyte contractile properties as described previously [29]. For HA rods, line scans were developed on myocytes with close proximity to the HA rods.

7.8 Infarct model and microrod injections

The animal protocol for induction of MI was approved by the Committee for Animal Research of the University of California San Francisco and was performed in accordance with the recommendations of the American Association for Accreditation of Laboratory Animal Care. The ischemia-reperfusion model used in this study has been extensively tested in our lab. All injections were performed successfully and there were no complications resulting from surgery or injection in any animal. Protocols were approved by the IACUC of UCSF.

To produce the MI model, female Sprague-Dawley rats (180–220g) underwent occlusion of the left anterior descending coronary artery for 30 minutes followed by reperfusion while under general anesthesia achieved by inhalation of 2% L/min isoflurane [53]. The chest was then closed and the animal was allowed to recover. The rats were randomized two days after MI to saline-injected, HA solution-injected, or microrod-injected treatment groups, and were given one intramuscular injection into the heart wall under blinded conditions via ultrasound guided transthoracic injection using a 29-gauge syringe [53]. Each injection consisted of 50 μL of sterile 0.9% sodium chloride solution (n=7), HA dissolved in sodium chloride solution at 4.2 mg/mL (n=9), or 50,000 of microrods in sodium chloride solution (n=7). Preliminary studies showed that 75 mg/mL HA microrods outperformed the 100 mg/mL microrods. 75 mg/mL HA microrods were used for all microrods injections presented in this study. Each injection was delivered to the center of the infarct region as visualized by hyperechoic signal on ultrasound. Successful injection was confirmed by a slight local increase in ultrasound signal in the vicinity of the syringe, as well as a brief thickening of the LV wall.

7.9 Echocardiography

Transthoracic echocardiography was performed with a 15-MHz linear array transducer system (Sequoia c256, Acuson, Erlangen, Germany) on all animals under 2% L/min isoflurane. Echocardiography was done prior to injection on day two post-MI and six weeks post-injection using standard methods that have been performed reproducibly in our lab

[24,53]. To determine left ventricular end diastolic volume (LVEDV), left ventricular end systolic volume (LVESV) and ejection fraction (EF) at 48 hours and six weeks, the ventricular shadow was outlined in both systole and diastole and the single plane area length algorithmic method was applied. Two-dimensional images were obtained in both parasternal long- and short-axis views at the papillary muscle level. Stroke volume (SV) was calculated by SV = LVEDV-LVESV, while change in EF was calculated by $\Delta EF = EF_{6\ weeks}\text{-}EF_{2\ days}$. Transverse images were obtained at three levels: basal (at the tip of the mitral valve leaflets), middle (at the papillary muscle level), and apical (distal to papillary muscle but before the cap of the cavity). All image analyses were performed in a blinded fashion. In cases where the ventricular shadow was not clearly identifiable in the 48 hour or six week image, the heart in question was excluded from echocardiographic analyses. Cases where ejection fraction was above 50% at 48 hours were excluded because they indicated an insufficient infarct model.

7.10 Histology

Sacrifice was performed after six weeks by maintaining the animal at 5% L/min isoflurane for five minutes, followed by bilateral thoracotomy and injection of potassium chloride into the right atrium to arrest the heart in diastole. The heart was then extracted and frozen in OCT (Sakura Finetech USA, Inc., Torrance, CA) on 2-methylbutane (Sigma Aldrich, St. Louis, MO) on dry ice and sectioned for histology and image analysis. Tissue blocks were cryo-sectioned at a thickness of 10 μm starting at the apex of the left ventricle and collecting 10 serial sections every 350 μm until 100 sections were collected. Sections were stained with H&E stains, Masson's Trichrome stain and Picrosirius red stains using standard protocols. For immunofluorescent stains, tissue sections were air dried and blocked with 10% serum, followed by incubation with primary and secondary antibodies using standard protocols. In brief, samples were incubated overnight with primary antibodies at 4°C in a solution of 0.1% Triton X-100, 0.05% Tween-20, 10% goat serum and 1% BSA in PBS (anti-vimentin, anti-CD68, anti-paxillin; Abcam, Cambridge, United Kingdom). After rinsing, secondary antibody was added for 45 minutes at room temperature. DAPI and AlexaFluor 546 phalloidin were added as a counterstain (Thermofisher, Waltham, MA).

7.11 Image Analysis

A Zeiss LSM 710 confocal microscope at UIC was used for fluorescence imaging of myocyte and fibroblast interactions with HA microrods *in vitro*. Single-plane and Z-stack images were obtained using a 63x Zeiss objective. Primary antibodies for paxillin [ab32084] and CD44 [ab157107] (Abcam, Cambridge, MA) were used at 1:250 and 1:1000 dilutions, respectively, incubated overnight, then counterstained with secondary antibody (A21207, Thermofisher, Waltham, MA), rhodamine phalloidin (R415, Thermofisher, Waltham, MA), and DAPI (H-1200, Vector Laboratories, Burlingame, CA).

Visualization of fibronectin bound to microrods was conducted by incubating HA microrods for 2 hr at 37°C in 10 μg/mL of fibronectin in PBS, or in PBS alone as a control. Fibronectin was eliminated by three cycles of centrifugation and resuspension in PBS. Microrods were incubated with a fibronectin antibody (ab26245, Abcam, Cambridge, MA) at a 1:1000 dilution for 1 hr at 37°C before centrifugation and resuspension in PBS three times; then,

microrods were incubated with fluorescently-labeled secondary antibody (A21202, Thermofisher, Waltham, MA) at a 1:400 dilution for 1 hr at room temperature before imaging in a fluorescence microscope.

For whole heart histology, images were taken using a Nikon 6D optical microscope (NIKON Instruments, Inc., Melville, NY) with 4–20x magnification (H&E, Masson's Trichrome, Picrosirius Red) and a Nikon spinning disc confocal microscope. All quantifications were performed using Nikon Elements. For wall thickness analysis, the minimum length across the infarct area was measured for each tissue section. The absolute minimum length across all available sections in a given heart sample was selected as the minimum wall thickness.

For collagen analysis, five sections of each heart were selected from throughout the coronal plane of the infarct zone and stained with picrosirius red to assess the distribution and density of collagen in the injured hearts. These sections were imaged under brightfield as well as under polarized light to visualize the collagen fibers. Infarct area was quantified and normalized to total area of the left ventricular free wall.

7.11 Statistical Analysis

All values for continuous variables are listed as the mean ± one standard deviation, unless otherwise indicated. *In vitro* and *in vivo* analysis was performed using a one-way analysis of variance (ANOVA), followed by multiple comparison by Holm-Sidak correction to identify differences between groups.

Supplementary Material

Refer to Web version on PubMed Central for supplementary material.

Acknowledgments

The authors would like to thank the UCSF Nikon Imaging center for the microscopy equipment and the UCSF Biomedical Micro and Nanofabrication Facility for use of photolithography equipment. We would also like to thank Jonathan Muncie from the Weaver Lab at UCSF for his assistance with the atomic force microscopy measurements. This research was made possible by funding support from the NIH (P01HL62426 and R01HL137209).

References

1. Wang H, Naghavi M, Allen C, Barber R, et al. Global, regional, and national life expectancy, all-cause mortality, and cause-specific mortality for 249 causes of death, 1980–2015: a systematic analysis for the Global Burden of Disease Study 2015. Lancet. 2016; 388:1459–1544. DOI: 10.1016/S0140-6736(16)31012-1 [PubMed: 27733281]
2. Peterson ED, Shah BR, Parsons L, Pollack CV, French WJ, Canto JG, Gibson CM, Rogers WJ. Trends in quality of care for patients with acute myocardial infarction in the National Registry of Myocardial Infarction from 1990 to 2006. Am Heart J. 2008; 156:1045–1055. DOI: 10.1016/j.ahj.2008.07.028 [PubMed: 19032998]
3. St MG, Sutton J, Sharpe N. Clinical Cardiology: New Frontiers Left Ventricular Remodeling After Myocardial Infarction Pathophysiology and Therapy. 2015:2981–2988.
4. Talman V, Ruskoaho H. Cardiac fibrosis in myocardial infarction—from repair and remodeling to regeneration. Cell Tissue Res. 2016; 365:563–581. DOI: 10.1007/s00441-016-2431-9 [PubMed: 27324127]

5. Nelson DM, Ma Z, Fujimoto KL, Hashizume R, Wagner WR. Intra-myocardial biomaterial injection therapy in the treatment of heart failure: Materials, outcomes and challenges. Acta Biomater. 2011; 7:1–15. DOI: 10.1016/j.actbio.2010.06.039 [PubMed: 20619368]
6. Tous E, Purcell B, Ifkovits JL, Burdick JA. Injectable acellular hydrogels for cardiac repair. J Cardiovasc Transl Res. 2011; 4:528–542. DOI: 10.1007/s12265-011-9291-1 [PubMed: 21710332]
7. Arnal-Pastor M, Chachques JC, Monleón Pradas M, Valles-Lluch A. Biomaterials for Cardiac Tissue Engineering. Intechopen. 2013; :275–323. DOI: 10.5772/56076
8. Hasan A, Khattab A, Islam MA, Hweij KA, Zeitouny J, Waters R, Sayegh M, Hossain MM, Paul A. Injectable Hydrogels for Cardiac Tissue Repair after Myocardial Infarction. Adv Sci. 2015; 2:1–18. DOI: 10.1002/advs.201500122
9. Zhu Y, Matsumura Y, Wagner WR. Ventricular wall biomaterial injection therapy after myocardial infarction: Advances in material design,mechanistic insight and early clinical experiences. Biomaterials. 2017; 129:37–53. DOI: 10.1016/j.biomaterials.2017.02.032 [PubMed: 28324864]
10. So JY, Yong HF, Choon HL, Bum SK, Ho SS, Park Y, Sun K. Regeneration of ischemic heart using hyaluronic acid-based injectable hydrogel. J Biomed Mater Res - Part B Appl Biomater. 2009; 91:163–171. DOI: 10.1002/jbm.b.31386 [PubMed: 19399850]
11. Ifkovits JL, Tous E, Minakawa M, Morita M, Robb JD, Koomalsingh KJ, Gorman JH, Gorman RC, Burdick Ja. Injectable hydrogel properties influence infarct expansion and extent of postinfarction left ventricular remodeling in an ovine model. Proc Natl Acad Sci. 2010; 107:11507–11512. DOI: 10.1073/pnas.1004097107 [PubMed: 20534527]
12. Tous E, Ifkovits JL, Koomalsingh KJ, Shuto T, Soeda T, Kondo N, JHG, Gorman RC, Burdick Ja. Influence of Injectable Hyaluronic Acid Hydrogel Degradation Behavior on Infarction Induced Ventricular Remodeling. Biomacromolecules. 2011; 12:4127–4135. DOI: 10.1021/bm201198x.Influence [PubMed: 21967486]
13. Abdalla S, Makhoul G, Duong M, Chiu RCJ, Cecere R. Hyaluronic acid-based hydrogel induces neovascularization and improves cardiac function in a rat model of myocardial infarction. Interact Cardiovasc Thorac Surg. 2013; 17:767–772. DOI: 10.1093/icvts/ivt277 [PubMed: 23851989]
14. Bonafè F, Govoni M, Giordano E, Caldarera C, Guarnieri C, Muscari C. Hyaluronan and cardiac regeneration. J Biomed Sci. 2014; 21:100.doi: 10.1186/s12929-014-0100-4 [PubMed: 25358954]
15. Rodell CB, Lee ME, Wang H, Takebayashi S, Takayama T, Kawamura T, Arkles JS, Dusaj NN, Dorsey SM, Witschey WRT, Pilla JJ, Gorman JH, Wenk JF, Burdick JA, Gorman RC. Injectable Shear-Thinning Hydrogels for Minimally Invasive Delivery to Infarcted Myocardium to Limit Left Ventricular Remodeling. Circ Cardiovasc Interv. 2016; 9doi: 10.1161/CIRCINTERVENTIONS.116.004058
16. Toole BP. Hyaluronan: from extracellular glue to pericellular cue. Nat Rev Cancer. 2004; 4:528–539. DOI: 10.1038/nrc1391 [PubMed: 15229478]
17. Jiang D, Liang J, Noble PW. Hyaluronan in Tissue Injury and Repair. Annu Rev Cell Dev Biol. 2007; 23:435–461. DOI: 10.1146/annurev.cellbio.23.090506.123337 [PubMed: 17506690]
18. Lee JY, Spicer AP. Hyaluronan: A multifunctional, megaDalton,stealth molecule. Curr Opin Cell Biol. 2000; 12:581–586. DOI: 10.1016/S0955-0674(00)00135-6 [PubMed: 10978893]
19. Itano N. Simple primary structure,complex turnover regulation and multiple roles of hyaluronan. J Biochem. 2008; 144:131–137. DOI: 10.1093/jb/mvn046 [PubMed: 18390876]
20. Huebener P, Abou-Khamis T, Zymek P, Bujak M, Ying X, Chatila K, Haudek S, Thakker G, Frangogiannis NG. CD44 is critically involved in infarct healing by regulating the inflammatory and fibrotic response. J Immunol. 2008; 180:2625–2633. 180/4/2625 [pii]. [PubMed: 18250474]
21. Chen WYJ, Abatangelo G. Functions of hyaluronan in wound repair. Wound Repair Regen. 1999; 7:79–89. DOI: 10.1046/j.1524-475X.1999.00079.x [PubMed: 10231509]
22. Allison DD, Grande-Allen KJ. Review. Hyaluronan: A Powerful Tissue Engineering Tool. Tissue Eng. 2006; 60913044658042. doi: 10.1089/ten.2006.12.ft-153
23. Burdick JA, Prestwich GD. Hyaluronic acid hydrogels for biomedical applications. Adv Mater. 2011; 23:41–56. DOI: 10.1002/adma.201003963
24. Pinney JR, Du KT, Ayala P, Fang Q, Sievers RE, Chew P, Delrosario L, Lee RJ, Desai TA. Discrete microstructural cues for the attenuation of fibrosis following myocardial infarction. Biomaterials. 2014; 35:8820–8828. DOI: 10.1016/j.biomaterials.2014.07.005 [PubMed: 25047625]

25. Allen J, Ryu J, Maggi A, Flores B, Greer JR, Desai T. Tunable Microfibers Suppress Fibrotic Encapsulation via Inhibition of TGFβ Signaling. Tissue Eng Part A. 2016; 22:142–150. DOI: 10.1089/ten.tea.2015.0087 [PubMed: 26507808]
26. Ayala P, Lopez JI, Desai TA. Microtopographical Cues in 3D Attenuate Fibrotic Phenotype and Extracellular Matrix Deposition: Implications for Tissue Regeneration. Tissue Eng Part A. 2010; 16:2519–2527. DOI: 10.1089/ten.tea.2009.0815 [PubMed: 20235832]
27. Bencherif SA, Srinivasan A, Horkay F, Hollinger JO, Matyjaszewski K, Washburn NR. Influence of the degree of methacrylation on hyaluronic acid hydrogels properties. Biomaterials. 2008; 29:1739–1749. DOI: 10.1016/j.biomaterials.2007.11.047 [PubMed: 18234331]
28. Cesaretti M, Luppi E, Maccari F, Volpi N. A 96-well assay for uronic acid carbazole reaction. 2003; 54:59–61. DOI: 10.1016/S0144-8617(03)00144-9
29. Broughton KM, Russell B. Cardiomyocyte subdomain contractility arising from microenvironmental stiffness and topography. Biomech Model Mechanobiol. 2015; 14:589–602. DOI: 10.1007/s10237-014-0624-2 [PubMed: 25273278]
30. Jessica L, Ungerleider KLC. Concise Review: Injectable Biomaterials for the Treatment of Myocardial Infarction and Peripheral Artery Disease: Translational ChallengesandProgress. Stem Cells Transl Med. 2014; 3:1090–1099. DOI: 10.5966/sctm.2014-0049 [PubMed: 25015641]
31. Hernandez MJ, Christman KL. Designing Acellular Injectable Biomaterial Therapeutics for Treating Myocardial Infarction and Peripheral Artery Disease. JACC Basic to Transl Sci. 2017; 2:212–226. DOI: 10.1016/j.jacbts.2016.11.008
32. Johnson TD, Christman KL. Injectable hydrogel therapies and their delivery strategies for treating myocardial infarction. Expert Opin Drug Deliv. 2013; 10:59–72. DOI: 10.1517/17425247.2013.739156 [PubMed: 23140533]
33. Discher DE. Tissue Cells Feel and Respond to the Stiffness of Their Substrate. Science (80-). 2005; 310:1139–1143. DOI: 10.1126/science.1116995
34. Cipitria A, Salmeron-Sanchez M. Mechanotransduction and Growth Factor Signalling to Engineer Cellular Microenvironments. Adv Healthc Mater. 2017; 6doi: 10.1002/adhm.201700052
35. Vogel V, Sheetz M. Local force and geometry sensing regulate cell functions. Nat Rev Mol Cell Biol. 2006; 7:265–275. DOI: 10.1038/nrm1890 [PubMed: 16607289]
36. Yeung T, Georges PC, Flanagan LA, Marg B, Ortiz M, Funaki M, Zahir N, Ming W, Weaver V, Janmey PA. Effects of substrate stiffness on cell morphology, cytoskeletal structure, and adhesion. Cell Motil Cytoskeleton. 2005; 60:24–34. DOI: 10.1002/cm.20041 [PubMed: 15573414]
37. Ingber DE. Cellular mechanotransduction: putting all the pieces together again. FASEB J. 2006; 20:811–827. DOI: 10.1096/fj.05 [PubMed: 16675838]
38. McNamara LE, Burchmore R, Riehle MO, Herzyk P, Biggs MJP, Wilkinson CDW, Curtis ASG, Dalby MJ. The role of microtopography in cellular mechanotransduction. Biomaterials. 2012; 33:2835–2847. DOI: 10.1016/j.biomaterials.2011.11.047 [PubMed: 22248989]
39. Baker DW, Tang L. Effect of microtopography on fibrocyte responses and fibrotic tissue reactions at the interface. ACS Symp Ser. 2012; 1120:339–353. DOI: 10.1021/bk-2012-1120.ch015
40. Jaalouk DE, Lammerding J. Mechanotransduction gone awry. Nat Rev Mol Cell Biol. 2009; 10:63–73. DOI: 10.1038/nrm2597 [PubMed: 19197333]
41. Humphrey JD, Dufresne ER, Schwartz MA. Mechanotransduction and extracellular matrix homeostasis. Nat Rev Mol Cell Biol. 2014; 15:802–812. DOI: 10.1038/nrm3896 [PubMed: 25355505]
42. Chopra A, Murray ME, Byfield FJ, Mendez MG, Halleluyan R, Restle DJ, Raz-Ben Aroush D, Galie PA, Pogoda K, Bucki R, Marcinkiewicz C, Prestwich GD, Zarembinski TI, Chen CS, Puré E, Kresh JY, Janmey PA. Augmentation of integrin-mediated mechanotransduction by hyaluronic acid. Biomaterials. 2014; 35:71–82. DOI: 10.1016/j.biomaterials.2013.09.066 [PubMed: 24120037]
43. Petrey AC, de la Motte CA. Hyaluronan, a crucial regulator of inflammation. Front Immunol. 2014; 5:1–13. DOI: 10.3389/fimmu.2014.00101 [PubMed: 24474949]
44. Khademhosseini A, Eng G, Yeh J, Fukuda J, Blumling J, Langer R, Burdick JA. Micromolding of photocrosslinkable hyaluronic acid for cell encapsulation and entrapment. J Biomed Mater Res - Part A. 2006; 79:522–532. DOI: 10.1002/jbm.a.30821

45. Kim Y, Kumar S. CD44-mediated adhesion to hyaluronic acid contributes to mechanosensing and invasive motility. Mol Cancer Res. 2014; 12:1416–29. DOI: 10.1158/1541-7786.MCR-13-0629 [PubMed: 24962319]

46. Bhattacharya DS, Svechkarev D, Souchek JJ, Hill TK, Taylor MA, Natarajan A, Mohs AM. Impact of structurally modifying hyaluronic acid on CD44 interaction. J Mater Chem B. 2017; 5:8183–8192. DOI: 10.1039/C7TB01895A [PubMed: 29354263]

47. Burdick JA, Chung C, Jia X, Randolph MA, Langer R. Controlled degradation and mechanical behavior of photopolymerized hyaluronic acid networks. Biomacromolecules. 2005; 6:386–391. DOI: 10.1021/bm049508a [PubMed: 15638543]

48. Leach JB, Bivens KA, Patrick CW, Schmidt CE. Photocrosslinked hyaluronic acid hydrogels: Natural, biodegradable tissue engineering scaffolds. Biotechnol Bioeng. 2003; 82:578–589. DOI: 10.1002/bit.10605 [PubMed: 12652481]

49. Cyphert JM, Trempus CS, Garantziotis S. Size Matters: Molecular Weight Specificity of Hyaluronan Effects in Cell Biology. Int J Cell Biol. 2015; 2015doi: 10.1155/2015/563818

50. Ruppert SM, Hawn TR, Arrigoni A, Wight TN, Bollyky PL. Tissue integrity signals communicated by highmolecular weight hyaluronan and the resolution of inflammation. Immunol Res. 2014; 58:186–192. DOI: 10.1007/s12026-014-8495-2 [PubMed: 24614953]

51. Gao F, Liu Y, He Y, Yang C, Wang Y, Shi X, Wei G. Hyaluronan oligosaccharides promote excisional wound healing through enhanced angiogenesis. Matrix Biol. 2010; 29:107–116. DOI: 10.1016/j.matbio.2009.11.002 [PubMed: 19913615]

52. Lin Y-H, Li J, Swanson ER, Russell B. CapZ and actin capping dynamics increase in myocytes after a bout of exercise and abates in hours after stimulation ends. J Appl Physiol. 2013; 114:1603–1609. DOI: 10.1152/japplphysiol.01283.2012 [PubMed: 23493359]

53. Mihardja SS, Gonzales JA, Gao D, Sievers RE, Fang Q, Stillson CA, Yu J, Peng M, Lee RJ. The effect of a peptide-modified thermo-reversible methylcellulose on wound healing and LV function in a chronic myocardial infarction rodent model. Biomaterials. 2013; 34:8869–8877. DOI: 10.1016/j.biomaterials.2013.07.028 [PubMed: 23895998]

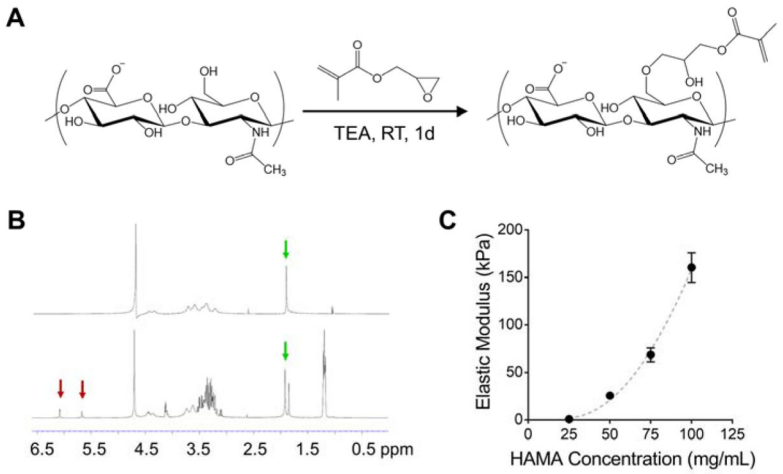

Figure 1. Synthesis and characterization of hyaluronic acid methacrylate

(A) Hyaluronic acid (100kDa) was reacted with glycidyl methacrylate to add photosensitive pendant groups to the polymer backbone. (B) ^{1}H-NMR was used to quantify the modification of HA (upper panel) with methacrylate groups (red arrows). The product (lower panel) had two methacrylate peaks at ~5.65 ppm and ~6.1 ppm, which was compared to the acetamide peak (green arrows) at 1.85 ppm to calculate the degree of substitution. (C) A range of concentrations of HA methacrylate were used to fabricate HA hydrogels with elastic moduli between 1 kPa and 160 kPa. The data indicate the mean ± SD (n=3 per group).

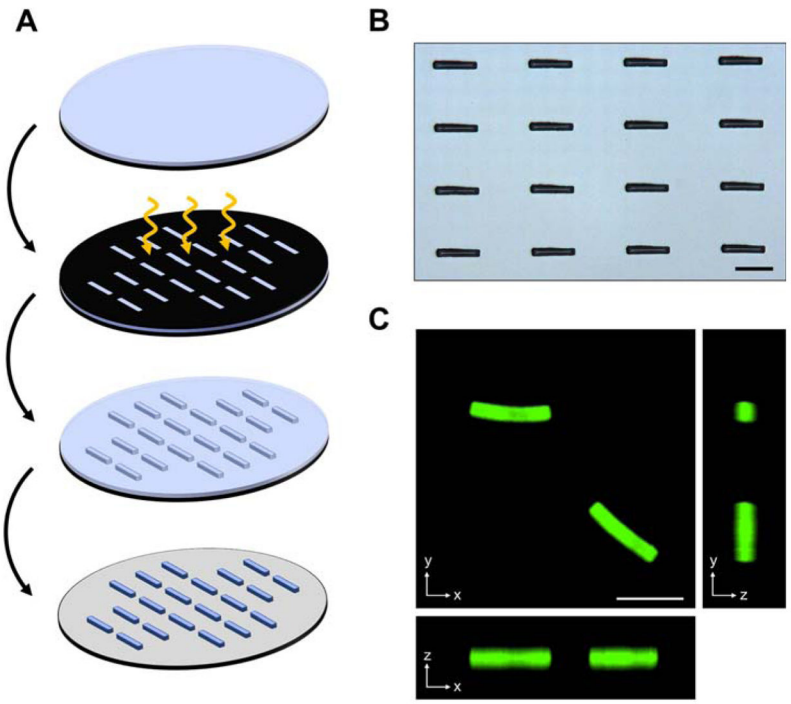

Figure 2. Microrod fabrication and characterization

(A) HA microrods were fabricated by exposure of a thin film of HA to UV light through a photomask and development in water. (B) Brightfield images of uniformly produced HA microrods on a silicon wafer. (C) Fluorescent images of HA microrods labeled with fluorescein show expected dimensions on all axes. Scale bars = 100 μm.

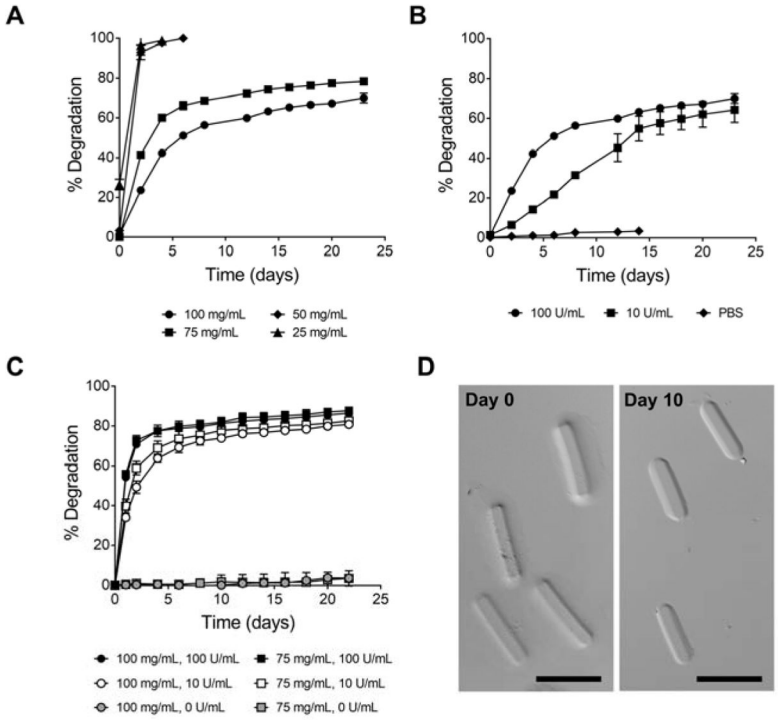

Figure 3. Surface Area and Crosslinking Density Affect Enzyme Mediated Degradation of Crosslinked HA

(A) HA hydrogels made from higher HAMA concentration have reduced rates of hyaluronidase-mediated degradation due to increased crosslinking density (n=3 per group). (B) 100 mg/mL HA hydrogels degraded in a range of hyaluronidase concentration suggesting biphasic degradation patterns consisting of enzyme degradation on accessible fragments on the surface. Hydrolysis creates new accessible fragments which are degraded by enzyme in the second, slower phase of degradation (100 U/mL: n=3, 10 U/mL: n=2, PBS: n=3) (C) Crosslinking density has limited effect on HA microrod degradation due to high surface area to volume ratio (n=3 per group). (D) Differential interference contrast (DIC) images of 100 mg/mL HA microrods incubated in 100 U/mL hyaluronidase for 10 days (right) demonstrates surface erosion of microrods. The data are presented as the mean ± SD. Scale bars = 100 μm.

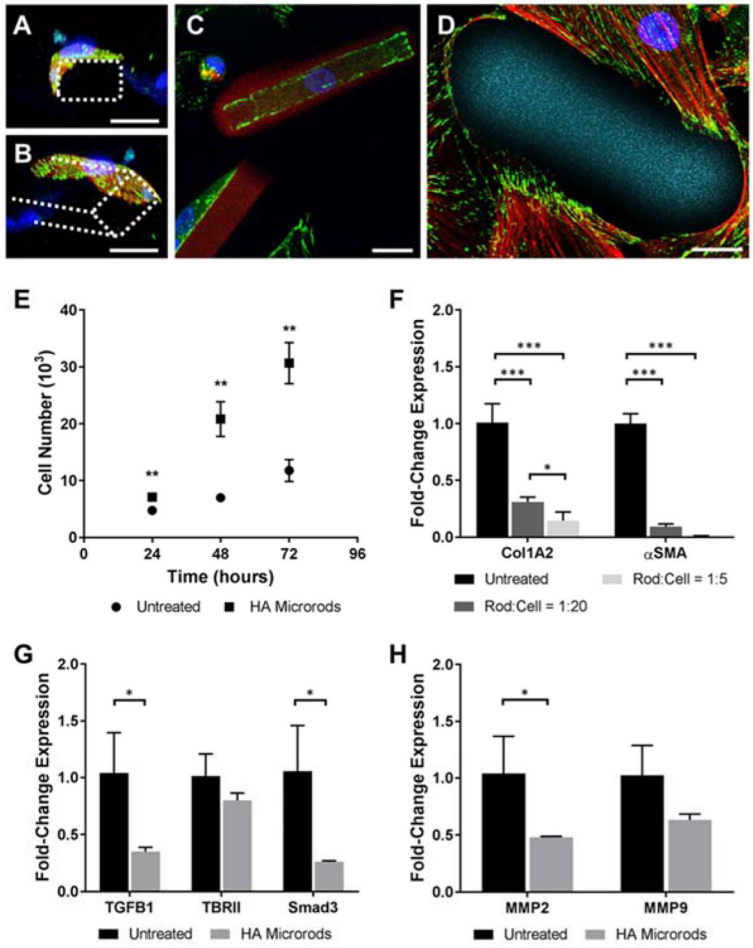

Figure 4. Fibroblasts interact with HA microrods *in vitro*

(A–D) Fluorescent immunocytochemical staining show that neonatal rat ventricular fibroblasts are highly interactive with HA microrods, actin (red), paxillin (green), nuclei (blue). Scale bars = 20 μm. (E) NIH-3T3 fibroblasts cultured with HA microrods have increased proliferation compared to control cells (n=3 per group). (F) NIH-3T3 fibroblasts exhibit dose-dependent reduction in Col1A2 and αSMA expression when cultured with HA microrods for 48 hours (n=3 per group). G) HA microrods reduce TGFβ1 and Smad3 expression in NIH-3T3 fibroblasts when cultured at a density of 1 rod per 5 cells. H) MMP2 expression is reduced in NIH-3T3 fibroblasts cultured with HA microrods at a density of 1 rod per 5 cells. The data are presented as the mean ± SD. $*p < 0.05$, $**p < 0.01$, $***p < 0.001$.

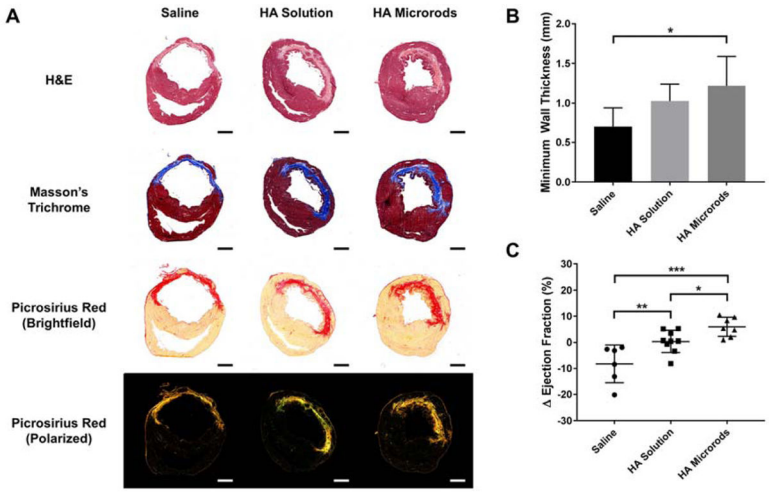

Figure 5. HA Microrods Reduce Left Ventricular Remodeling and Improve Functional Outcomes after MI

(A) Cardiac tissue sections were stained with H&E, Masson's Trichrome and Picrosirius red to visualize cell infiltration, vascularization and scar tissue formation. Scale bars = 2 mm. (B) Left ventricular wall thinning was significantly reduced in hearts treated with HA microrods (n=6) compared to saline injection (n=7). Hearts treated with HA solution had moderate but insignificant wall thinning (n=8). (C) Echocardiography was used to compare the ejection fraction (EF) 2 days after MI (immediately prior to injection) and 6 weeks after injection in rats treated with saline (n=6), soluble HA (n=9) and HA microrods (n=7). Rats treated with HA microrods have significantly higher change in EF over rats treated with saline or HA solution. The data are presented as the mean ± SD. *$p < 0.05$, **$p < 0.01$, ***$p < 0.001$.

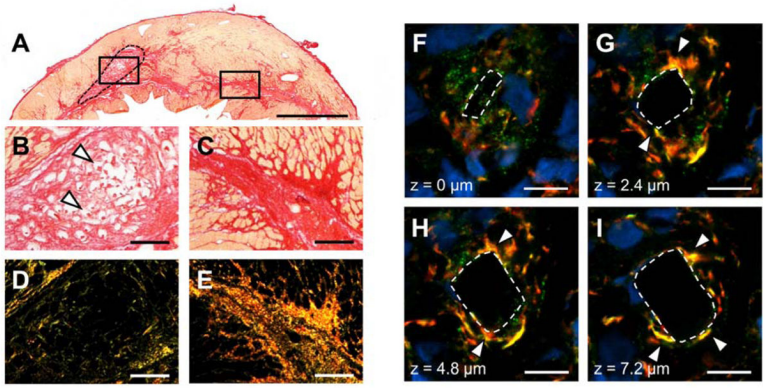

Figure 6. HA microrods interact with fibroblasts *in vivo* and locally reduce collagen deposition

(A–E) A representative Picrosirius red stained section of a HA treated heart. The dotted shape indicates the injection site. Collagen around the injection site (B,D) was sparse compared to far away from the injection site (C,E). The collagen near the microrods (white arrows) is loose and does not appear under polarized light, while the collagen away from the injection site matures into dense bundles. Scale bars = 2 mm (A) and 200 μm (B–E). (F–I) Confocal images of microrods show that cells interact closely with HA microrods *in vivo*. Cells formed distinct focal adhesions (white arrow) along the edges of the microrods. Tissues were stained for nuclei (blue), actin (red) and paxillin (green). Scale bars = 20 μm.